

Submitted to the Astronomical Journal

## X-ray properties of the quasar HE0450-2958

Xin-Lin Zhou<sup>1,2</sup>, Fang Yang<sup>1,2</sup>, Xiao-Rong Lü<sup>1,2</sup>, Jian-Min Wang<sup>1</sup>

### ABSTRACT

We present an *XMM-Newton* EPIC observation of HE0450-2958 which may be a “naked” quasar as suggested by Magain et al. The *XMM-Newton* EPIC spectra show a substantial soft X-ray excess, a steep photon index, as well as marginal evidence for a weak Fe K $\alpha$  line. The X-ray absorption is consistent with the galactic level. The 0.3-10 keV EPIC spectra can be fitted by a power law plus a blackbody model, however, the fit by the relativistically blurred photoionized disc reflection is better. We estimate the black hole mass of  $2_{-1.3}^{+7} \times 10^7 M_\odot$  from the X-ray variability. This broadly agrees with the value derived from the optical H $\beta$  line width. These results support a high-state Seyfert galaxy of the source. HE0450-2958 shares similar properties of transitional objects from ultra-luminous infrared galaxies to quasars. We suggest that HE0450-2958 is just in the beginning of an optical quasar window.

*Subject headings:* infrared: galaxies- galaxies: individual: HE0450-2958- galaxies: active - X-rays: galaxies

### 1. INTRODUCTION

HE0450-2958 is a bright quasar ( $z = 0.285$ ) located  $\sim 1.5''$  from an ultra-luminous infrared galaxy (ULIRG) and revealed by the *Hubble* space telescope (Boyce et al. 1996; Canalizo & Stockton 2001). Recently, there have been controversies on the nature of HE0450-2958 (Magain et al. 2005; Merritt et al. 2006; Haehnelt et al. 2006; Hoffman & Loeb 2006). HE0450-2958 resides in an elliptical galaxy. Assuming that the quasar is accreting at half the Eddington limit with a radiative efficiency of 10%, Magain et al. (2005) inferred the

---

<sup>1</sup>Key Laboratory for Particle Astrophysics, Institute of High Energy Physics, Chinese Academy of Sciences, Beijing 100049, China

<sup>2</sup>Graduate School of Chinese Academy of Sciences, Beijing 100049, China

mass of the central supermassive black hole (SMBH) of  $8 \times 10^8 M_\odot$  from the quasar absolute magnitude  $M_V = -25.8$ . They argued that the host galaxy luminosity is at least 6 times fainter than that predicted from the relation between the SMBH mass and the host-galaxy spheroid luminosity (Mclure & Dunlop 2002). They thus concluded that the quasar’s host galaxy is dark, or the quasar is “naked”. This suggests the possible evidence for the ejection of a SMBH from a galaxy merger event (Haehnelt et al. 2006; Hoffman & Loeb 2006).

However, Merritt et al. (2006) presented the optical spectra to argue that HE0450-2958 is a narrow-line Seyfert 1 galaxy (NLS1). They derived the SMBH mass of  $(2-11) \times 10^7 M_\odot$  from the  $H\beta$  line width. Then the inferred host-galaxy luminosity from the SMBH mass is consistent with the observed luminosity. They also argued that the ejection model (Haehnelt et al. 2006; Hoffman & Loeb 2006) can be ruled out since the narrow emission line gas remains bound to the SMBH as showed by the quasar’s optical spectra.

The controversies lie in the host nature and the SMBH mass of the quasar. X-ray observations, as a powerful probe of the SMBH activities (Mushotzky et al. 1993), may provide independent clues to understand the nature of the source. Here we present an *XMM-Newton* observation of the X-ray counterpart of HE0450-2958. We find that it is a high-state Seyfert 1 galaxy, i.e., accreting above the Eddington limit. Throughout this paper, we use the cosmological parameters of  $H_0 = 70 \text{ km s}^{-1} \text{ Mpc}^{-1}$ ,  $\Omega_m = 0.3$ ,  $\Omega_\Lambda = 0.7$ .

## 2. DATA REDUCTION

HE0450-2958 was observed by *XMM-Newton* on 2003 Sep.9 during orbit 687 (PI: N. Anabuki). The observational details of the European Photon Imaging Camera (EPIC) on-board *XMM-Newton*, including the two MOS cameras (Turner et al. 2001) and the pn camera (Strüder et al. 2001) can be seen in Table 1.

The cookbook for the *XMM-Newton* data analysis software SAS in the *XMM-Newton* Data Center at MPE <sup>1</sup> is referred for the data reduction. The EPIC data are screened with the

---

<sup>1</sup><http://wave.xray.mpe.mpg.de/xmm/cookbook>

Table 1: Instrument modes and exposure times.

Ins.	Mode	filter	time(ksec)
MOS 1	Full Frame	medium	15.7
MOS 2	Full Frame	medium	15.7
pn	Full Frame	medium	14.0

SAS v6.0 software (Gabriel et al. 2004), and the corresponding calibration files are available<sup>2</sup>. The X-ray events corresponding to patterns 0-4 (single and double pixel events) for the pn data and patterns 0-12 for the MOS data are selected. The EPIC data are used in the 0.3 - 10 keV range and hot or bad pixels are removed. We extract the source spectra from a circle within 38"(760 pixels) of the detected source position, with the background being taken from a circular source-free region with the same size avoiding the CCD chip gaps. The presence of background flaring in the observation has been checked and removed via using a Good Time Interval (GTI) file, leaving 13.1 ks for the pn and 15.2 ks for the MOS. We find no pile-ups in the EPIC data after checking by the SAS task *epatplot*. The response files are generated with the SAS tools *rmfgen* and *arfgen*. Spectral files are binned to at least 20 counts per bin to apply the  $\chi^2$  statistics. Spectral fit is based on the XSPEC v12.3.0 package (Arnaud 1996). Errors are quoted at the 90% confidence level ( $\Delta\chi^2 = 2.71$ ).

The X-ray source is located at 04<sup>h</sup>52<sup>m</sup>30<sup>s</sup>.2,  $-29^\circ 53' 34''.6$  (J2000.0). Note that EPIC has a spatial resolution of  $\sim 10''$  or worse (Ghizzardi et al. 2001), however, the quasar is  $\sim 1.5''$  apart from the ULIRG. Thus, the HE0450-2958 system can't be resolved spatially by EPIC. All the fits include the absorption due to the line-of-sight Galactic column of  $N_{\text{H}} = 1.68 \times 10^{20} \text{ cm}^{-2}$  (Dickey & Lockman 1990), and fitting parameters are given in the rest-frame.

### 3. Results

#### 3.1. Temporal analysis

##### 3.1.1. excess variance

We extract the 2-10 keV EPIC pn light curve with the time bin of 256 s, the same as adopted by O'Neill et al. (2005). The count rates show evident variations in  $\sim$  ks timescale (Fig. 1). To quantify the X-ray variability of HE0450-2958, we invoke the X-ray excess variance denoted as  $\sigma_{\text{rms}}^2$  (Nandra et al. 1997 and Turner et al. 1999),

$$\sigma_{\text{rms}}^2 = \frac{1}{N\mu^2} \sum_{i=1}^N [(X_i - \mu)^2 - \sigma_i^2], \quad (1)$$

where  $X_i$  is the count rates for the  $N$  points in the light curve, with the errors  $\sigma_i$ .  $\mu$  is the arithmetic mean of  $X_i$ . The errors of  $\sigma_{\text{rms}}^2$ , which depend on the measurement uncertainties

---

<sup>2</sup> <http://xmm.vilspa.esa.es/ccf>

and the stochastic nature of the source, can be expressed as (O’Neill et al. 2005),

$$\Delta_{\text{tot}}(\sigma_{\text{rms}}^2) = \sqrt{\left(\frac{\sigma_{\text{frac}}\sigma_{\text{rms}}^2}{\sqrt{N_{\text{seg}}}}\right)^2 + [\Delta_{\text{boot}}(\sigma_{\text{rms}}^2)]^2}, \quad (2)$$

where  $N_{\text{seg}}$  is the number of available light-curve segments,  $\sigma_{\text{frac}}$  is a fractional standard deviation,  $\sigma_{\text{frac}} = 0.74$  for  $\log M_{\text{BH}} > 6.54$  and  $\sigma_{\text{frac}} = 0.48$  for  $\log M_{\text{BH}} < 6.54$ .  $\Delta_{\text{boot}}(\sigma_{\text{rms}}^2)$  is the bootstrap uncertainty which comes from the bootstrap simulation accounting for the measurement uncertainties. We find that  $\sigma_{\text{rms}}^2 = 0.0081 \pm 0.0063$  from the 2-10 keV EPIC pn data. We don’t use the EPIC MOS data since the MOS data have much lower count rates with relatively larger errors.

### 3.1.2. Time lag

We calculate the cross-correlation function (CCF) between the light curves of 0.3-2 keV and 2-10 keV with the time bin of 50 s (Fig. 2). The CCF is obtained using the XRONOS command CROSSCOR, which uses a direct Fourier method to compute the coefficient. Errors are obtained via propagating the errors of the concerned light curves through the cross correlation formulae. The results show the hard X-ray to be no lagging with respect to the soft X-ray emission.

## 3.2. Spectral analysis

### 3.2.1. Power law

We use all the EPIC data (pn+MOS1+MOS2) for the spectral analysis to improve the photon statistics allowing tighter constraints on spectral parameters. Initially we use a power law to fit the data above 1 keV with a free intrinsic absorption. A good fit can be obtained ( $\chi^2_v$  of 1.06 for 521 d.o.f.), with the intrinsic absorption consistent with zero. A substantial soft X-ray excess below 1 keV can be seen in the EPIC pn and MOS data when extrapolating this power law over the full energy range of EPIC (Fig. 3).

We use the models listed in Table 2 to fit 0.3 - 10 keV spectrum. The soft X-ray excess is traditionally taken as thermal emission (e.g. Pounds et al. 1995). Model 1 is an absorbed power law plus a blackbody model. This gives an acceptable fit over the full energy range ( $\chi^2_v$  of 1.17 for 747 d.o.f., Model 1 in Table 2), with the photon index of  $2.13^{+0.04}_{-0.03}$ . There are some evidences for an absorption gap between 0.7-0.8 keV in the spectra. We add an

Table 2: Spectral fits to the combined EPIC (pn+MOS1+MOS2) data

Model <sup>a</sup>	$\Gamma$	$N_{\text{H}}^{\text{int}}$ ( $10^{20} \text{ cm}^{-2}$ )	$kT_{BB}$ (eV)	$N_{BB}$ ( $\times 10^{-5}$ )	$E_{\text{edge}}$ (eV)	$\tau$	$E_{K\alpha}$ (keV)	$EW_{K\alpha}$ (eV)	$\theta$	$\log \xi$	$\chi^2/d.o.f.$
(1)	(2)	(3)	(4)	(5)	(6)	(7)	(8)	(9)	(10)	(11)	(12)
1.	$2.13^{+0.04}_{-0.03}$	$< 0.03$	$99^{+3}_{-2}$	$9.7^{+3.4}_{-0.5}$	-	-	-	-	-	-	872.8/747
2.	$2.16^{+0.03}_{-0.03}$	$< 0.01$	$107^{+5}_{-8}$	$7.5^{+0.7}_{-0.4}$	$773^{+34}_{-18}$	$0.29^{+0.07}_{-0.11}$	-	-	-	-	845.0/745
3.	$2.16^{+0.03}_{-0.03}$	$< 0.01$	$106^{+6}_{-6}$	$7.7^{+1.4}_{-0.6}$	$776^{+29}_{-19}$	$0.26^{+0.09}_{-0.07}$	$6.40^f$	$< 64$	-	-	842.2/744
4.	$2.15^{+0.04}_{-0.04}$	$< 0.01$	-	-	$788^{+31}_{-29}$	$0.38^{+0.08}_{-0.07}$	$6.40^f$	$< 36$	$42^{+8}_{-10}$	$3.2^{+0.3}_{-0.1}$	798.1/738
5.	$2.35^{+0.02}_{-0.02}$	$< 0.01$	-	-	$759^{+11}_{-13}$	$0.49^{+0.06}_{-0.07}$	$6.40^f$	$< 42$	$38^{+10}_{-8}$	$3.4^{+0.2}_{-0.2}$	849.2/741
					$1190^{+30}_{-40}$	$0.30^{+0.07}_{-0.08}$					

Note. -(1): model; (2): photon index; (3): intrinsic column density; (4): blackbody temperature; (5) blackbody normalization; (6) energy of absorption edge; (7) optical depth of absorption edge; (8) energy of Fe  $K\alpha$  line; (9) equivalent width of Fe  $K\alpha$  line; (10) inclination angle in the reflection model of PEXRIV; ] (11) ionization parameter in PEXRIV. <sup>a</sup> Model expressed in XSPEC command. 1: phabs \* zphabs (powerlaw+zbody); 2: phabs \* zphabs zedge (powerlaw+zbody); 3: phabs \* zphabs \* zedge (powerlaw+zbody+zgauss); 4: phabs \* zphabs \* zedge (kdblur (powerlaw+atable {reflion.mod})+zgauss); 5: phabs \* zphabs \* zedge \* zedge (pexriv+zgauss). <sup>f</sup> fixed.

absorption edge to Model 1. This improves the fit significantly ( $\Delta\chi^2$  of 27.8 for 2 fewer d.o.f., Model 2). We find that the edge significance is at the level of  $> 99.9\%$  by applying the  $F$ -test. It should be due to the absorption edge of O VII in 739 eV (Reynolds 1997). The second absorption edge due to O VIII is not required in this model ( $\Delta\chi^2$  of 1.2 for 2 fewer d.o.f. when including the second absorption edge).

### 3.2.2. Fe $K$ line

We first try to add a Gaussian line with all free parameters. However, this fit does not improve significantly ( $\Delta\chi^2$  of 2.7 for 3 fewer d.o.f.). Since the Fe  $K\alpha$  lines in current data are generally narrow (Nandra 2006), we fix the intrinsic width of the line at 10 eV. This fit is still poor ( $\Delta\chi^2$  of 2.6 for 2 fewer d.o.f.), and the line energy can not be constrained well. We also fix the line energy at 6.40 keV. This returns an equivalent width of  $< 64$  eV. The line significance  $F^{\text{line}}$  is at a level of 89% compared to the continuum alone. Generally, the significance should be larger than 90% for the presence of a Fe  $K\alpha$  line. Thus, the line is barely significant.

### 3.2.3. soft X-ray excess

Recently, it has been suggested that the soft X-ray excess can be arised from a relativistically blurred photoionized disc reflection in a large sample of AGNs (Crummy et al. 2006). The relativistic convolution KDBLUR has been included in XSPEC v12.3.0 and the

photoionized disc reflection model of REFLION (Ross & Fabian 2005) is also available <sup>3</sup>. We follow Crummy et al. (2006), fix the outer radius of accretion disc at  $100 R_g$ . This fit (Model 4) is better than the blackbody fit of Model 3 ( $\Delta\chi^2$  of 44.1 for 6 fewer d.o.f., see Table 2), with the inner radius of the accretion disc at  $1.6^{+0.6}_{-0.2} R_g$ , the index of the emissivity of the accretion disc of  $8.1^{+1.9}_{-3.5}$ , the iron abundance of the accretion disc of  $0.4^{+0.1}_{-0.2}$  (relative to solar), the photon index for illuminating power-law spectrum of  $2.38^{+0.03}_{-0.02}$ . Other parameters in this model have been listed in Table 2.

We further test the reflection scenario by using the PEXRIV model (Magdziarz & Zdziarski 1995) to fit 0.3-10 keV spectrum. Although the PEXRIV model doesn't include the relativistically blurring effect, it can generally represent the reflection from the ionized material. We fix the high-energy cutoff at 200 keV, the reflector at unity (Malizia et al. 2003). This fit is worse than the blackbody model ( $\Delta\chi^2$  of -7 for 3 fewer d.o.f. ), but still acceptable ( $\chi^2_v$  of 1.15 for 741 d.o.f.).

## 4. Discussion

### 4.1. BH mass

We calculate the black hole (BH) mass based on the anti-correlation between the X-ray excess variance  $\sigma_{\text{rms}}^2$  and the BH mass (Lu & Yu 2001; Bian & Zhao 2003; Papadakis 2004; O'Neill et al. 2005). Using the correlation derived from Eq. 3 in O'Neill et al. (2005),

$$\log M_{\text{BH}} = 5.75 + 1.20 \log \left( \frac{0.144}{\sigma_{\text{rms}}^2} - 1 \right), \quad (3)$$

we obtain the BH mass of  $2^{+7}_{-1.3} \times 10^7 M_{\odot}$  (Fig. 7).

We plot the spectral energy distribution (SED) for HE0450-2958 in Fig. 8. There is a “Big Blue Bump”(BBB) in the UV band. We fit the BBB with a standard thin accretion disk model (Döerrer et al. 1996) and fit the X-ray data with a power law plus a blackbody model. The accretion disk fit (dotted line in Fig. 8) returns a large BH mass of  $8 \times 10^8 M_{\odot}$ , with the Eddington ratio of 0.3, the inclination angle  $\cos\theta = 0.5$  and the BH spin parameter  $a = 0.6$ . This BH mass is much higher than our result. It is possible that the UV and optical data is contaminated by the nearby ULIRG and thus the SED luminosity is overestimated. A similar case appears in NLS1 Ton S180, the estimation of BH mass based on the SED from the simultaneous multiple band observations is also much higher than that from the H $\beta$  line

---

<sup>3</sup><http://heasarc.gsfc.nasa.gov/docs/xanadu/xspec/models/reflion.html>

width (Turner et al. 2002). Alternatively, it is not a reliable way to estimate the BH masses in NLS1s by fitting SED using a standard thin disk model, since they may accrete above the Eddington limit and the standard thin disk model does not work in this case (Kawaguchi et al. 2004). It is worth studying the SED of HE0450-2958 through more sophisticated slim disk model (Abramowicz et al. 1988; Wang et al. 1999) in future.

#### 4.2. Eddington ratio

The X-ray excess variance is related with the observed X-ray luminosity  $L_X$  and the Eddington ratio  $\mathcal{E} \equiv L_{\text{bol}}/L_{\text{Edd}}$  through (Leighly 1999),

$$\sigma_{\text{rms}}^2 \propto \left( \frac{L_X}{\eta \mathcal{E}} \right)^{1-\alpha}, \quad (4)$$

where  $L_{\text{bol}}$  is the bolometric luminosity and  $L_{\text{Edd}}$  is the Eddington luminosity,  $\eta$  is the radiation efficiency and  $\alpha$  is the slope of the power spectrum, assuming  $\alpha = 2$  (Leighly 1999). The integrated  $2 - 10$  keV flux of HE0450-2958 is  $2.00 \times 10^{-12}$  ergs  $\text{s}^{-1}$   $\text{cm}^{-2}$ , corresponding to a luminosity of  $5.13 \times 10^{44}$  ergs  $\text{s}^{-1}$ . We find that HE0450-2958 is located in the NLS1 region in the  $\sigma_{\text{rms}}^2 - L_X$  plot of Leighly (1999), indicating that HE0450-2958 has a high Eddington ratio. This supports the hypothesis that HE0450-2958 is a NLS1 galaxy.

The soft and the hard X-rays in HE0450-2958 can arise from very close regions. As suggested above, a slim disk may be powering HE0450-2958. The fluctuations of the slim accretion disk can be the origin of the simultaneous X-rays variations (Mineshige et al. 2000; Wang & Netzer 2003). In this case, the slim disk suffers the so-called “photon bubble instability” (Gammie 1998) since the energy densities of the trapped photons and the magnetic field are larger than those in standard accretion disks. This leads to the hard X-rays closely following the soft X-rays variations. The zero lag between the soft and the hard X-rays in HE0450-2958 supports this scenario.

The yielded hard photon index of  $2.16^{+0.03}_{-0.03}$ , is steeper than the average photon index of  $1.8 - 2.0$  in Seyfert 1 galaxies (Nandra & Pounds 1994; George et al. 2000) and in quasars (Reeves & Turner 2000). The AGNs with steep X-ray indices as well as the strong soft X-ray emission have been considered as high-state objects (Pounds et al. 1995). According to the anti-correlation between the FWHM ( $H\beta$ ) and the hard X-ray index (Brandt et al. 1997), the FWHM ( $H\beta$ ) of HE0450-2958 should be narrow, also consistent with a NLS1.

The hard X-ray photon index is related to Eddington ratio (e.g. Shemmer et al. 2006). We calculate  $\mathcal{E}$  from the  $\Gamma_{2-10\text{keV}} - \mathcal{E}$  relation in Wang et al. (2004),

$$\Gamma_{2-10\text{keV}} = 2.05 + 0.26 \log \mathcal{E}. \quad (5)$$

We find  $\mathcal{E} = 3_{-1}^{+1}$  for  $\Gamma_{2-10\text{keV}} = 2.16 \pm 0.03$ . This suggests that HE0450-2958 is accreting above the Eddington limit.

The AGN bolometric luminosity can be estimated from the X-ray luminosity by multiplying the bolometric correction  $f_{\text{bol/x}}$ . We find the bolometric luminosity to be  $9_{-6}^{+16} \times 10^{45}$  ergs s $^{-1}$  by assuming  $f_{\text{bol/x}} = 17_{-11}^{+33}$ . The  $f_{\text{bol/x}}$  we used is the range in conversion factors that the bolometric luminosity accounts for the X-ray luminosity found in Elvis et al. (1994), also consistent with recent estimation by Marconi et al. (2004) and Barger et al. (2005). We then estimate the BH mass of  $2_{-1.2}^{+5} \times 10^7 M_{\odot}$  for  $L_{\text{bol}} = 9_{-6}^{+16} \times 10^{45}$  ergs s $^{-1}$  and  $\mathcal{E} = 3$ , agreeing with the  $M_{\text{BH}}$  from the X-ray variability.

The weak Fe K $\alpha$  emission can be also due to the high Eddington ratio (Pounds et al. 2003) for the anti-correlation between the equivalent width of narrow Fe K $\alpha$  line and Eddington ratio (Zhou & Wang 2005).

### 4.3. On the origin of Soft X-ray excess

The origin of the soft X-ray excess is still under debate. The traditional view is that the soft X-ray excess is the high-energy tail of BBB which is the thermal emission from the inner region of the accretion disc. The inferred Eddington ratio ( $\mathcal{E} = 3_{-1}^{+1}$ ), is too high for a standard accretion disk. The slim disc can be applied for the super-Eddington accretion. The effective temperature of the slim disc can be written as (Wang & Netzer 2003),

$$T_{\text{eff}} = 3.14 \times 10^3 \gamma_0^{-1/4} M_{\text{BH}}^{-1/4} (r/r_s)^{-1/2} \text{ eV}, \quad (6)$$

where  $\gamma_0 = (5 + \alpha^2/2)^{1/2}$  is a weak function of the viscosity  $\alpha$ ,  $\gamma_0 \approx 2.24$  for  $\alpha \ll 1$ . We find  $T_{\text{eff}} \approx 23$  eV for  $r = 3r_s$  and  $M_{\text{BH}} = 2 \times 10^7 M_{\odot}$ . However, the derived blackbody temperature from the spectral fitting,  $kT_{BB} = 106 \pm 6$  eV, is much higher than expected. For the thermal origin of the soft X-ray excess, it is difficult to reconcile the BH mass to the blackbody temperature (e.g., a slim disc temperature 100 eV requires a BH mass of  $< 10^5 M_{\odot}$ ). However the innermost region of accretion disk may be very complicated, such as strong outflow developed from the disk itself, evidenced by PG 1211+143 (Pounds & Page 2006). Comptonization inside the outflow has not been studied, but might significantly contribute to the soft X-ray excess. Actually the temperature holds a constant in the transition layer between the hot corona and cold disk, it may also have important contribution to the soft X-ray excess (Nayakshin & Melia 1997). As noted by Gierliński & Done (2004), many AGNs with quite different BH masses have soft X-ray excess with the temperature confined in a very narrow range. This points out towards an atomic nature (either related to absorption or reflection) for the soft excess, rather than a thermal origin.

Whereas the blackbody model can fit the spectra, our result shows that the fit by relativistically blurred disc reflection model is better. This supports that the soft X-ray excess can arise from the disc reflection. The ionization parameter given by the reflection model is large ( $\log \xi = 3.2_{-0.1}^{+0.3}$ ), implying that the reflection material is highly ionized. The simulation of X-ray photoionized accretion disc shows that the surface of the accretion disc can be significantly ionized at a high Eddington ratio (Matt et al. 1993). The highly-ionized disc surface becomes reflective in the soft X-ray band, producing a steepening X-ray continuum (Haardt & Maraschi 1993; Nayakshin et al. 2000; Ballantyne et al. 2001). This scenario is physically plausible for HE0450-2958.

#### 4.4. X-ray properties of the transitionary objects

Canalizo & Stockton (2001) compiled a sample (including HE0450-2958) of low-redshift ( $z \leq 0.4$ ) objects that are in a transitionary stage between ULIRGs and quasars. Their sample selected from the intermediate position in the far-infrared color-color diagram between the regions occupied by the two classes of objects from the IRAS all-sky survey is nearly complete. We collect the X-ray data of Canalizo & Stockton (2001) sample given in Table 3. For seven X-ray detected objects, all show steep X-ray photon indices and small X-ray intrinsic absorption, with the exception of Mrk 231, which is heavily obscured. Thus HE0450-2958 is very similar to other objects.

In the hierarchical formation paradigm, quasars are formed and fueled via galaxy-galaxy mergers (Kauffmann & Haehnelt 2000; Di Matteo et al. 2005). During the major merger of two comparable galaxies, the quasar is dust-enshrouded and the SMBH growth is obscured by the gas funneled toward a merger nucleus. This picture is supported by a new population of submm and hard X-ray sources at  $z \approx 1.5 - 3$  (Chapman et al. 2003; Alexander et al. 2005). When SMBH reaches a critical mass, the feedback from the SMBH activity expels gas, and cleans the obscuring material (Silk & Rees 1998; Fabian 1999; Ciotti & Ostriker 2001). The detailed simulation of galaxy mergers shows that this process creates a window in which the SMBH is observable as an optical quasar for the duration of  $\sim 10 - 20$  Myr for a  $B$ -band luminosity greater than  $10^{11} L_\odot$  (Hopkins et al. 2005). We argue that HE0450-2958 is just in the beginning of the optical quasar window for: 1) the small X-ray intrinsic absorption, implying that the AGN is dust-cleaned and optical-visible; 2) the high accretion rate inferred from the steep X-ray index and the NLS1 nature; 3) the relatively smaller BH mass compared with the optical-selected quasars (Hao et al. 2005; Kawakatu et al. 2006).

The IR luminosities of ULIRGs denote the intense bursts of star formation and also the “violence” of interactions and mergers (Sanders & Mirabel 1996). The steep X-ray photon indices of AGNs denote the super-Eddington accretion of SMBHs. These ULIRGs associated with AGNs with steep X-ray indices shed new light on the coeval growth of the stellar bulges and SMBHs in the hierarchical paradigm.

## 5. Conclusions

The *XMM-Newton* EPIC spectra of HE0450-2958 show a substantial soft X-ray excess, a steep photon index, as well as marginal evidence for a weak Fe  $K\alpha$  line. The X-ray absorption is consistent with the galactic level. The 0.3-10 keV EPIC spectra can be fitted by a power law plus a blackbody model, however, the fit by the relativistically blurred photoionized disc reflection is better. We estimate the black hole mass of  $2_{-1.3}^{+7} \times 10^7 M_\odot$  from the X-ray variability. This broadly agrees with the value derived from the optical  $H\beta$  line width. These results support a high-state Seyfert galaxy of the source.

HE0450-2958 shares similar properties of transitional objects from ultra-luminous infrared galaxies to quasars. we suggest that HE0450-2958 is just in the beginning of the optical quasar window.

We are grateful to an anonymous referee for the constructive comments and help with English. W.-H. Bian, Z.-H. Fan, F. Zhang and Y.-M. Chen are thanked for reading the manuscript. We also appreciate the discussion among people in IHEP AGN group. This

research is supported by NSFC through NSFC-10325313, 10233030 and 10521001.

## REFERENCES

Abramowicz, M. A., Czerny, B., Lasota, J. P., & Szuszkiewicz, E. 1988, *ApJ*, 332, 646

Alexander, D. M., Smail, I., Bauer, F. E., Chapman, S. C., Blain, A. W., Brandt, W. N., & Ivison, R. J. 2005, *Nature*, 434, 738

Arnaud, K. A. 1996, *ASPC*, 101, 17

Ballantyne, D. R., Ross, R. R., & Fabian, A. C. 2001, *MNRAS*, 323, 506

Barger, A. J., Cowie, L. L., Mushotzky, R. F., Yang, Y., Wang, W. H., Steffen, A. T., & Capak, P. 2005, *AJ*, 129, 578

Bian, W.-H., & Zhao, Y.-H. 2003, *MNRAS*, 343, 164

Boyce, P. J. et al. 1996, *ApJ*, 473, 760

Braito, V. et al. 2004, *A&A*, 420, 79

Brandt, W. N., Mathur, S., & Elvis, M. 1997, *MNRAS*, 285, L25

Canalizo, G., & Stockton, A. 2001, *ApJ*, 555, 719

Chapman, S. C., Blain, A. W., Ivison, R. J., & Smail, I. R. 2003, *Nature*, 422, 695

Ciotti, L., & Ostriker, J. P. 2001, *ApJ*, 551, 131

Crummy, J., Fabian, A. C., Gallo, L., & Ross, R. R. 2006, *MNRAS*, 365, 1067

Dickey, J. M., & Lockman, F. J. 1990, *ARA&A*, 28, 215

Di Matteo, T., Springel, V., & Hernquist, L. 2005, *Nature*, 433, 604

Döerrer, T., Riffert, H., Staubert, R., & Ruder, H. 1996, *A&A*, 311, 69

Elvis, M. et al. 1994, *ApJS*, 95, 1

Fabian, A. C. 1999, *MNRAS*, 308, L39

Gabriel, C. et al. 2004, *ASPC*, 314, 759

Gammie, C. F. 1998, *MNRAS*, 297, 929

George, I. M., Turner, T. J., Yaqoob, T., Netzer, H., Laor, A., Mushotzky, R. F., Nandra, K., & Takahashi, T. 2000, *ApJ*, 531, 52

Ghizzardi S. et al. 2001, In flight calibration of the PSF for the MOS1 and MOS2 cameras, EPIC-MCT-TN-011

Gierliński, M., & Done, C. 2004, *MNRAS*, 349, L7

Haardt, F., & Maraschi, L. 1993, *ApJ*, 413, 507

Haehnelt, M. G., Davies, M. B., & Rees, M. J. 2006, *MNRAS*, 366, L22

Hao, C.-N., Xia, X.-Y., Mao, S.-D., Wu, H., & Deng, Z.-G. 2005, *ApJ*, 625, 78

Imanishi, M., & Terashima, Y. 2004, *AJ*, 127, 758

Hoffman, L., & Loeb, A. 2006, *ApJ*, 638, L75

Hopkins, P. F., Hernquist, L., Martini, P., Cox, T. J., Robertson, B., Di Matteo, T., & Springel, V. 2005, *ApJ*, 625, L71

Kauffmann, G., & Haehnelt, M. 2000, *MNRAS*, 311, 576

Kawaguchi, T., Pierens, A., & Huré, J. M. 2004, *A&A*, 415, 47

Kawakatu, N., Anabuki, N., Nagao, T., Umemura, M., & Nakagawa, T. 2006, *ApJ*, 637, 104

Letawe, G., Magain, P., Courbin, F., Jablonka, P., Jahnke, K., Meylan, G., & Wisotzki, L. 2006, *MNRAS(astro-ph/0605288)*

Leighly, K. M. 1999, *ApJS*, 125, 297

Lu, Y. J., & Yu, Q. J. 2001, *MNRAS*, 324, 653

Magain, P., Letawe, G., Courbin, F., Jablonka, P., Jahnke, K., Meylan, G., & Wisotzki, L. 2005, *Nature*, 437, 381

Magdziarz, P., & Zdziarski, A. A. 1995, *MNRAS*, 273, 837

Malizia, A., Bassani, L., Stephen, J. B., Di Cocco, G., Fiore, F., & Dean, A. J. 2003, *ApJ*, 589, L17

Marconi, A., Risaliti, G., Gilli, R., Hunt, L. K., Maiolino, R., & Salvati, M. 2004, *MNRAS*, 351, 169

Matt, G., Fabian, A. C., & Ross, R. R. 1993, MNRAS, 262, 179

McLure, R. J., & Dunlop, J. S. 2002, MNRAS, 331, 795

Merritt, D., Storchi-Bergmann, T., Robinson, A., Batcheldor, D., Axon, D., & Roberto, C. F. 2006, MNRAS, 367, 1746

Mineshige, S., Kawaguchi, T., Takeuchi, M., & Hayashida, K. 2000, PASJ, 52, 499

Mushotzky, R. F., Done, C., & Pounds, K. A. 1993, ARA&A, 31, 717

Nandra, K., & Pounds, K. A. 1994, MNRAS, 268, 405

Nandra, K., George, I. M., Mushotzky, R. F., Turner, T. J., & Yaqoob, T. 1997, ApJ, 476, 70

Nandra, K. 2006, MNRAS, 368, L62

Nayakshin, S., Kazanas, D., & Kallman, T. R. 2000, ApJ, 537, 833

Nayakshin, S., & Melia, F. 1997, ApJ, 484, L103

O'Neill, P. M., Nandra, K., Papadakis, I. E., & Turner, T. J. 2005, MNRAS, 358, 1405

Papadakis, I. E. 2004, MNRAS, 348, 207

Piconcelli, E., Jimenez-Bailn, E., Guainazzi, M., Schartel, N., Rodrguez-Pascual, P. M., & Santos-Lle, M. 2005, A&A, 432, 15

Pounds, K. A., Done, C., & Osborne, J. P. 1995, MNRAS, 277, L5

Pounds, K. A., Reeves, J. N., Page, K. L., Wynn, G. A., & O'Brien, P. T. 2003, MNRAS, 342, 1147

Pounds, K. A., & Page, K. L. 2006, MNRAS, preprint (astro-ph/0607099)

Ross, R. R., & Fabian, A. C. 2005, MNRAS, 358, 211

Reeves, J. N., & Turner, M. J. L. 2000, MNRAS, 316, 234

Reynolds, C. S. 1997, MNRAS, 286, 513

Sanders, D. B., & Mirabel, I. F. 1996, ARA&A, 34, 749

Scott, J. E., Kriss, G. A., Brotherton, M., Green, R. F., Hutchings, J., Shull, J. M., & Zheng, W. 2004, ApJ, 615, 135

Siemiginowska, A., Aldcroft, T. L., Bechtold, J., Brunetti, G., Elvis, M., & Stanghellini, C. 2003, PASA, 20, 113

Shemmer, O., Brandt, W. N., Netzer, H., Maiolino, R., & Kaspi, S. 2006, ApJ, 646, L29

Silk, J., & Rees, M. J. 1998, A&A, 331, L1

Strüder, L. et al. 2001, A&A, 365, L18

Turner, M. J. L. et al. 2001, A&A, 365, L27

Turner, T. J., George, I. M., Nandra, K., & Turcan, D. 1999, ApJ, 524, 667

Turner, T. J., et al. 2002, ApJ, 568, 120

Wang, J.-M., & Netzer, H. 2003, A&A, 398, 927

Wang, J.-M., Szuszkiewicz, E., Lu, F.-J., & Zhou, Y.-Y. 1999, ApJ, 522, 839

Wang, J.-M., Watarai, K.-Y., & Mineshige, S. 2004, ApJ, 607, L107

Zhou, X.-L., & Wang, J.-M. 2005, ApJ, 618, L83

Table 3: The transitional objects in Canalizo & Stockton (2001)

Name	$z$	$\log L_{\text{IR}}$ ( $L_{\odot}$ )	$\Gamma_{2-10\text{keV}}$	$N_{\text{H}}^{\text{int}}$ ( $10^{22} \text{ cm}^{-2}$ )	Ref.
I Zw1	0.061	11.97	$2.31_{-0.03}^{+0.03}$	$0.09_{-0.02}^{+0.02}$	1
3C48	0.367	13.02	$1.96_{-0.04}^{+0.04}$	$< 0.21$	4
IR 07598+6508	0.148	12.54	$2.9_{-0.5}^{+0.6}$	$0.08_{-0.06}^{+0.1}$	5
Mrk 231	0.042	12.55	$2.48_{-0.11}^{+0.20}$	$265_{-85}^{+173}$	6
F00275-2859	0.279	12.71	-	-	-
PG 1700+518	0.292	12.70	X-ray	undetected	3
HE 0450-2958	0.285	12.72	$2.16_{-0.03}^{+0.03}$	$< 0.01$	2
PG 1543+489	0.400	12.78	$2.64_{-0.20}^{+0.19}$	$0.07_{-0.07}^{+0.11}$	3
Mrk 1014	0.163	12.63	$2.24_{-0.07}^{+0.06}$	0.	1

Ref. for X-ray data: 1. Piconcelli et al. (2005);  
2. this work; 3. George et al. (2000); 4. Siemiginowska et al. (2003); 5. Imanishi & Terashima (2004); 6. Braito et al. (2004).

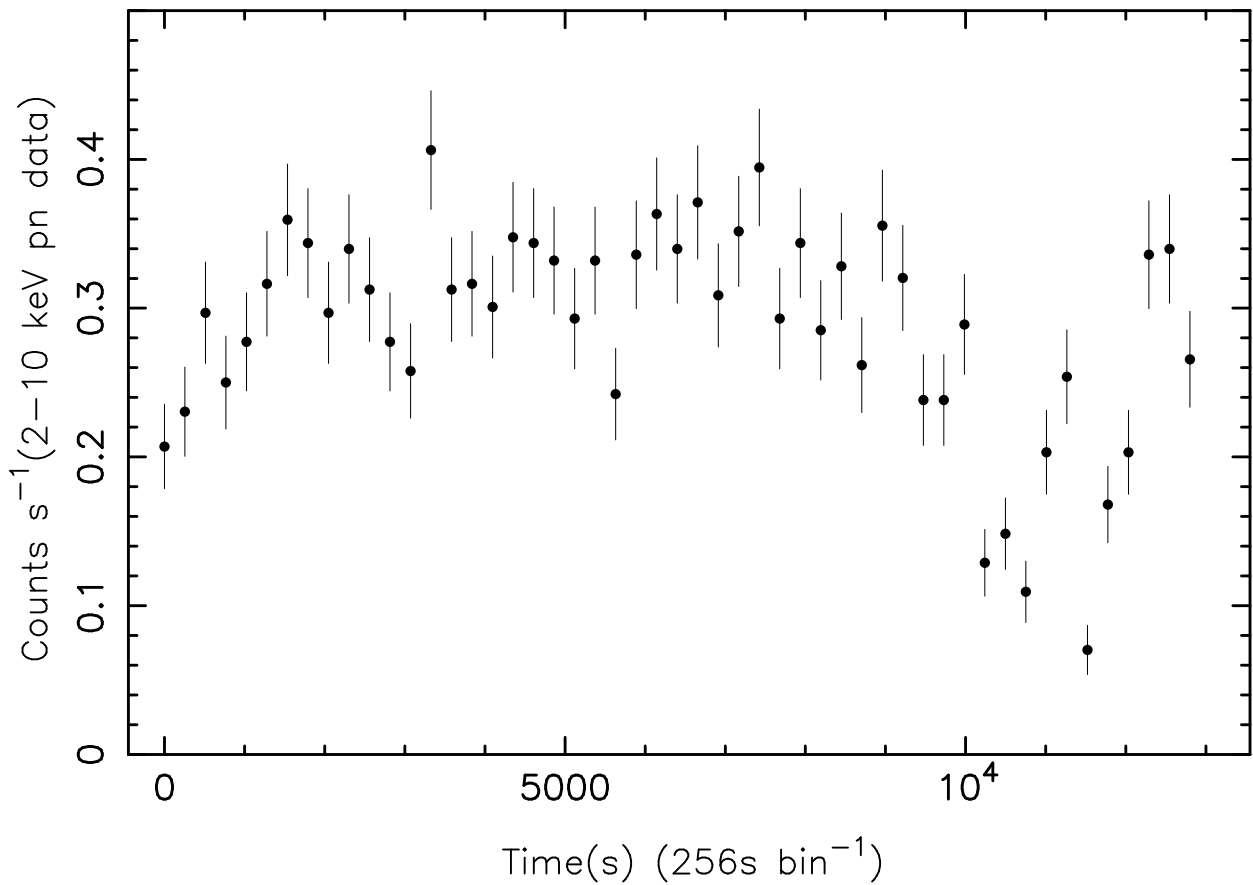


Fig. 1.— The 2-10 keV EPIC pn light curve of HE0450-2958 with the time bin of 256 s shows the rapid variability.

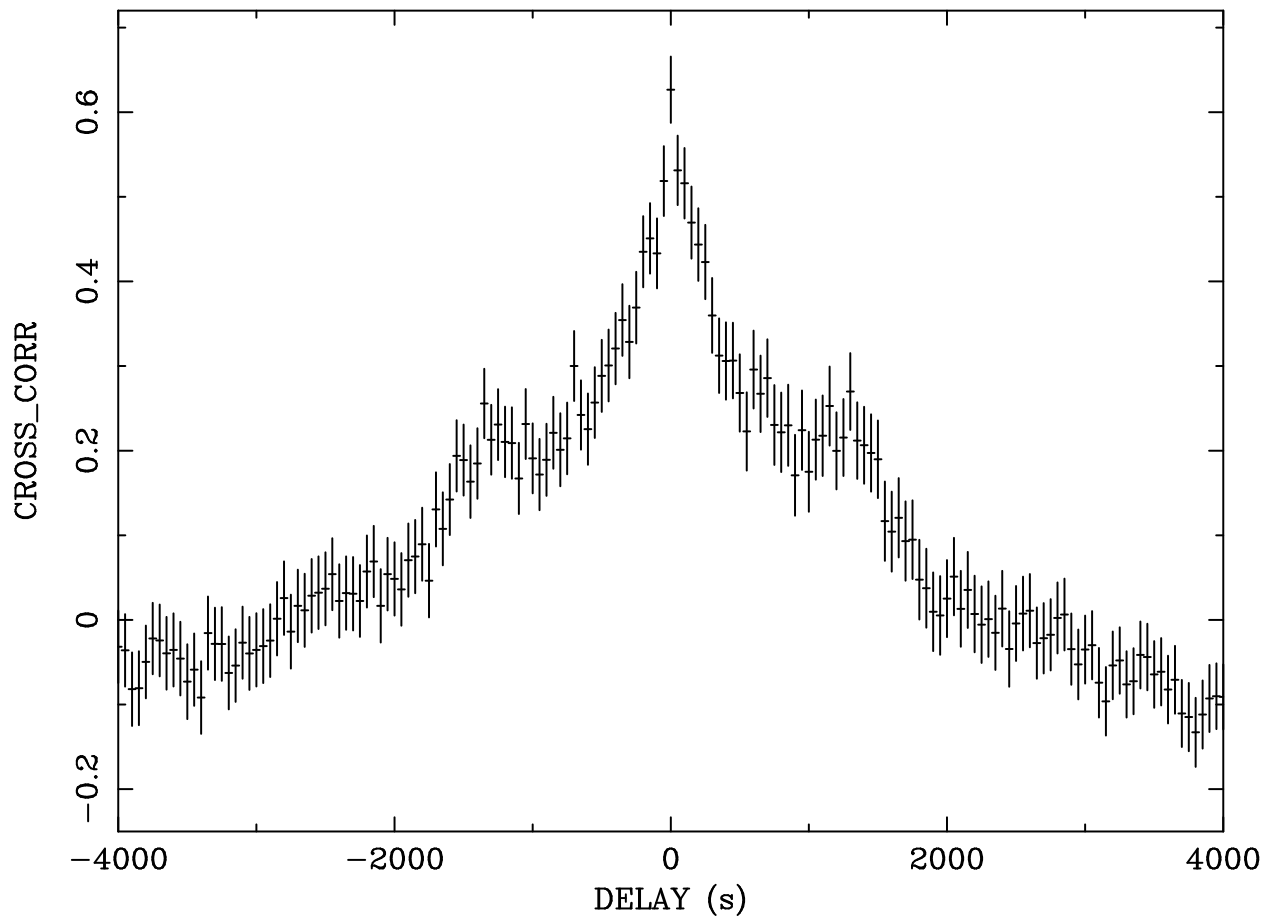


Fig. 2.— The cross-correlation function between the light curves of 0.3-2 keV and 2-10 keV with the time bin of 50 s shows no time lag between these two X-ray bands.

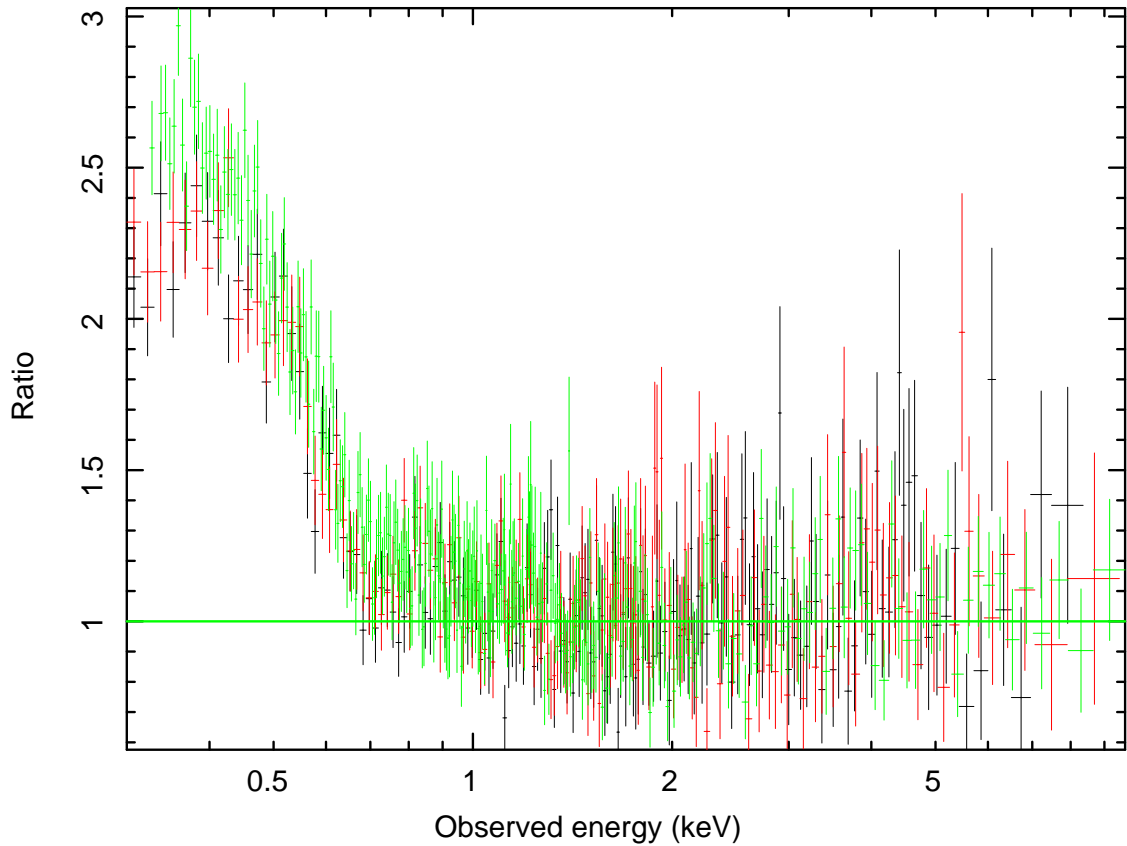


Fig. 3.— The EPIC pn (green), MOS1 (black) and MOS2 (red) spectra of HE0450-2958. The data is fitted with a simple power law over 1-10 keV, index  $\Gamma = 2.14 \pm 0.03$ . A soft X-ray excess is clear seen below 1 keV.

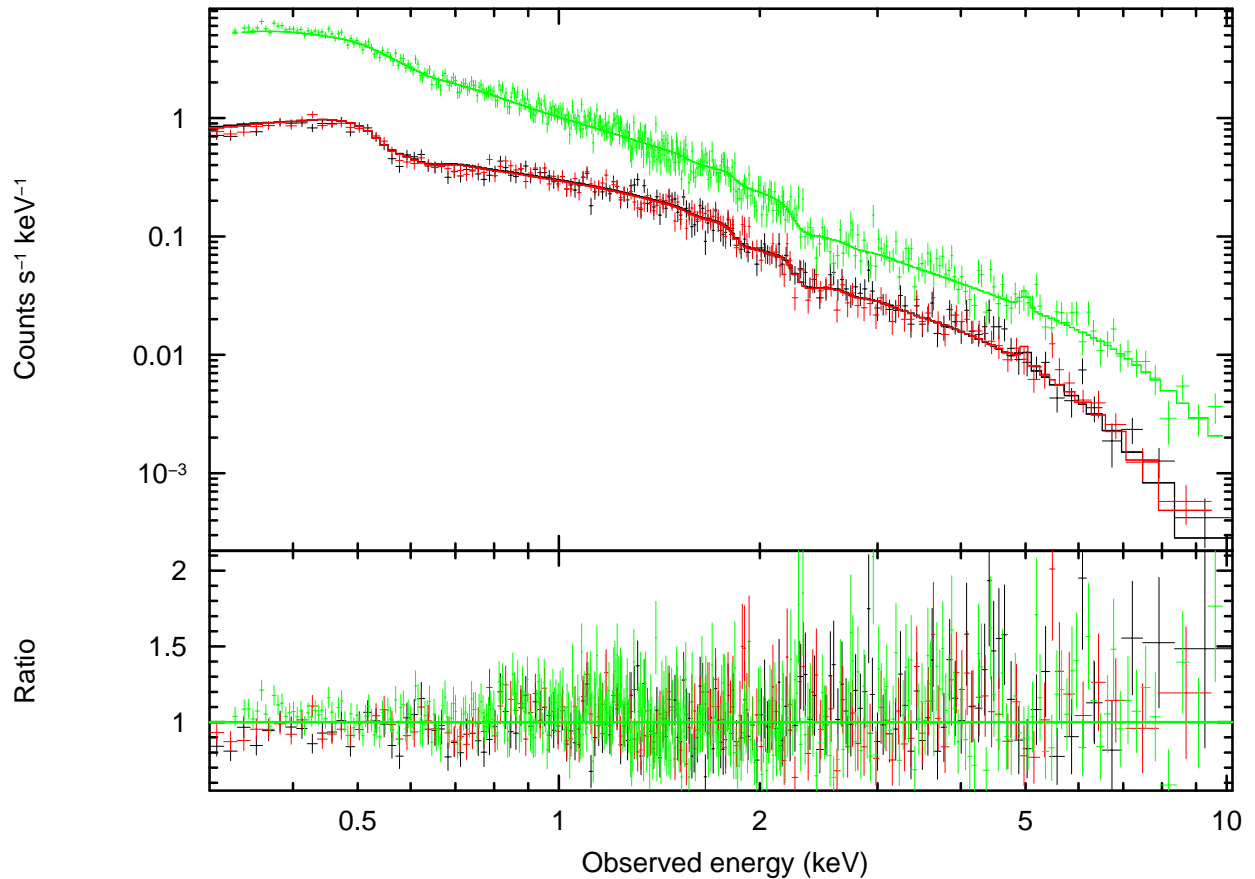


Fig. 4.— The power law plus blackbody model fit to the EPIC pn (green), MOS1 (black) and MOS2 (red) data ( $\chi^2_v$  of 1.13 for 744 d.o.f., Model 3 in Table 2). This model also includes a narrow Gaussian and an absorption edge.

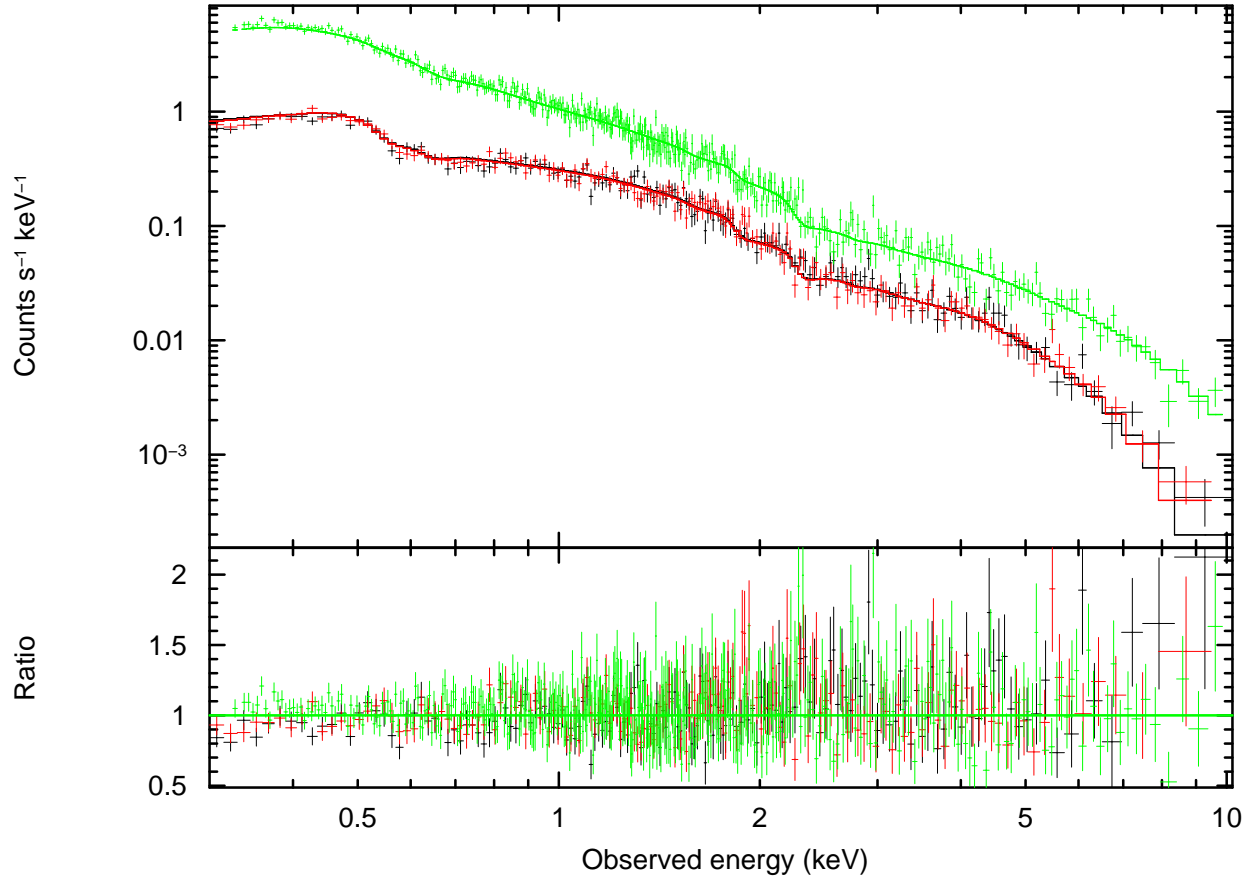


Fig. 5.— The relativistically blurred photoionized disc reflection fit to the EPIC pn (green), MOS1 (black) and MOS2 (red) data (Model 4 in Table 2). This model also includes a narrow Gaussian and an absorption edge. The fit is statistically better than the blackbody fit ( $\Delta\chi^2$  of 44.1 for 6 fewer d.o.f.) and physically plausible.

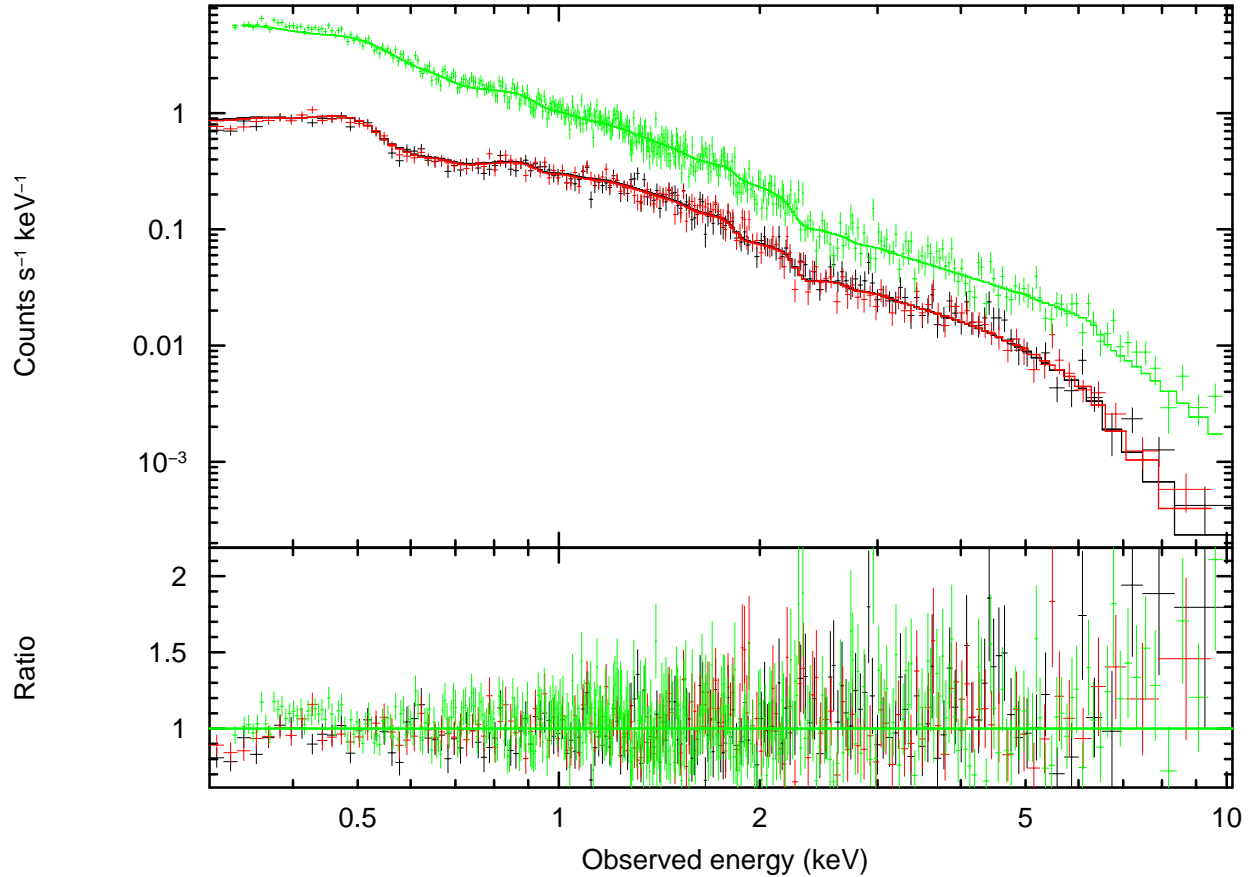


Fig. 6.— The reflection model of PEXRIV fit to the EPIC pn (green), MOS1 (black) and MOS2 (red) data (Model 5 in Table 2). This model also includes two absorption edges and a narrow Gaussian. The fit is worse than the blackbody fit ( $\Delta\chi^2$  of -7 for 3 fewer d.o.f. ), but still acceptable ( $\chi^2_v$  of 1.15 for 741 d.o.f.).

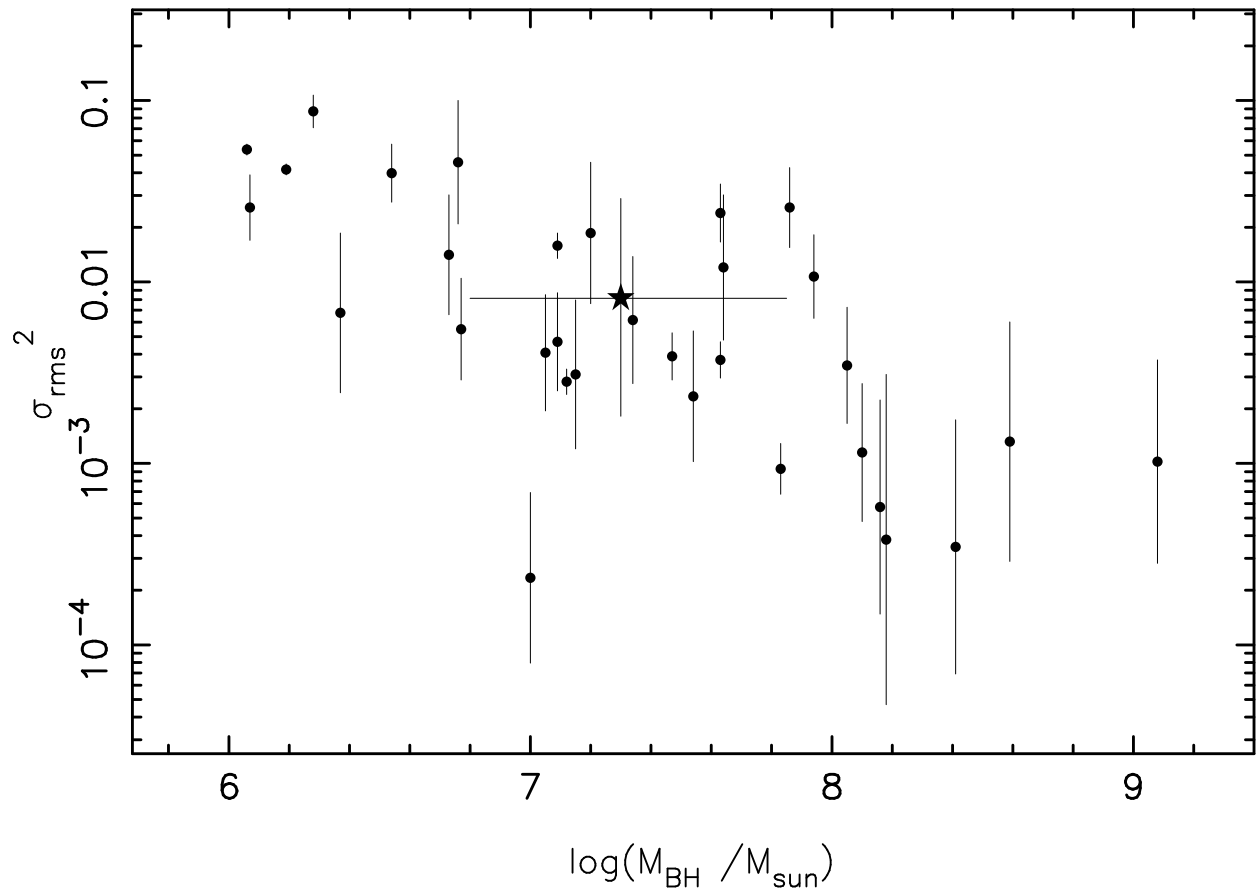


Fig. 7.— The X-ray excess variance  $\sigma_{\text{rms}}^2$  against the BH mass. The filled circles are taken from O'Neill et al. (2005), the pentacle indicates our result of HE0450-2958.

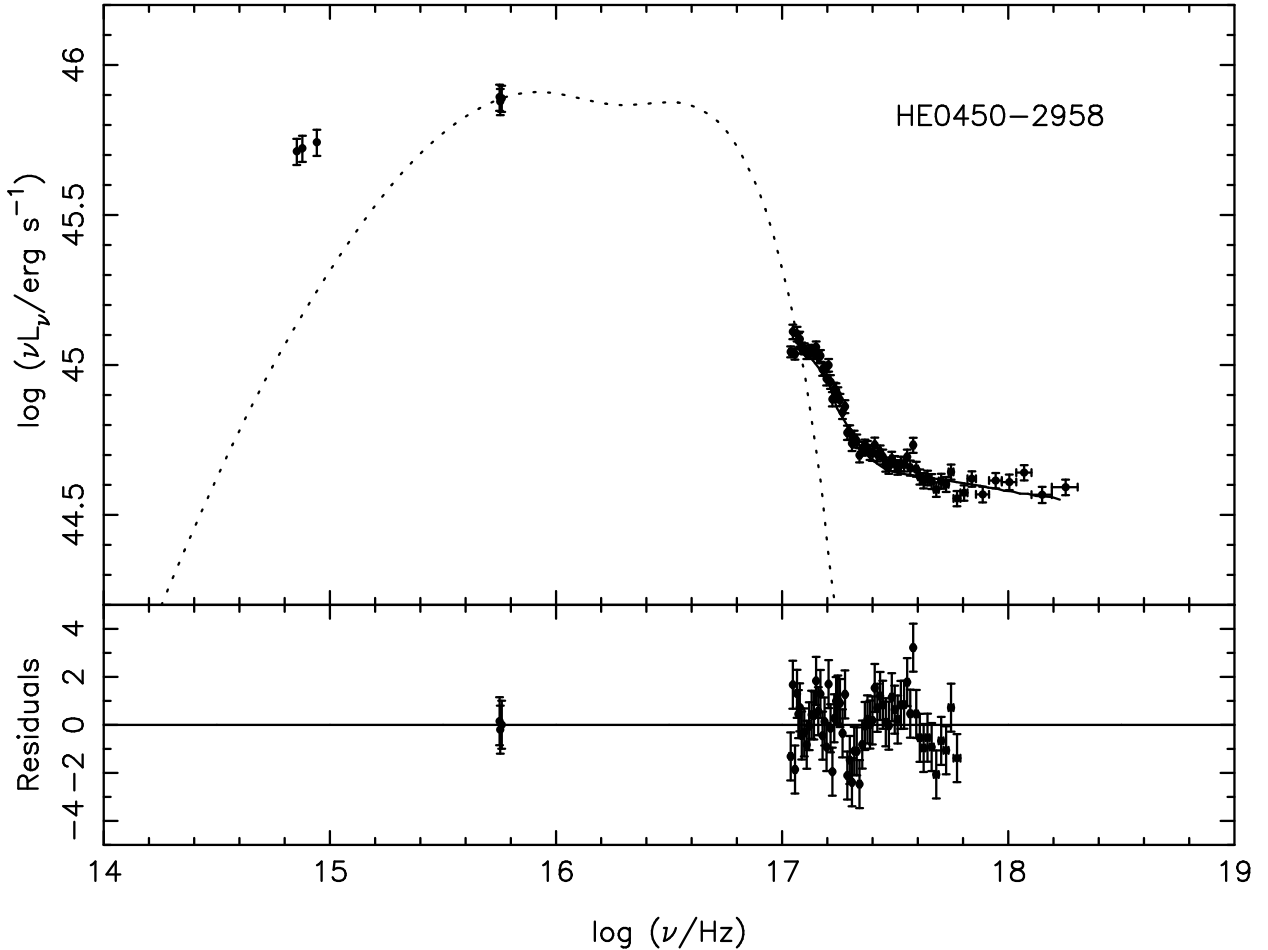


Fig. 8.— The spectral energy distribution of HE0450-2958 shows a big blue bump in the UV band. The UV and optical data are taken from Scott et al. (2004) and Letawe et al. (2006), respectively. A standard thin accretion disk model is used to fit the UV bump (dotted line). This gives a BH mass of  $8 \times 10^8 M_\odot$  with an Eddington ratio of 0.3, the inclination angle  $\cos\theta = 0.5$  and the BH spin parameter  $a = 0.6$ . This mass is much higher than the estimation from the X-ray variability. The X-ray data are fitted with a power law plus a blackbody model (solid line).